Journal of Achievements in Materials and Manufacturing Engineering
VOLUME 33
ISSUE 1
March
2009

Half-shaft undercarriage systems – designing and operating problems

E. Rusiński *, J. Czmochowski, P. Moczko
Institute of Machines Design and Operation, Wroclaw University of Technology,
ul. Lukasiewicza 7/9 , 51-370 Wrocław, Poland
* Corresponding author: E-mail address: eugeniusz.rusinski@pwr.wroc.pl

Received 04.06.2007; published in revised form 01.03.2009

Analysis and modelling

ABSTRACT

Purpose: The paper discuss designing and operating problems of half-shafts undercarriage systems of open pit machines. Example of failure of such system and investigation of its reasons are presented.
Design/methodology/approach: Experimental and numerical methods were used to investigate reasons of dumping conveyor breakdown. In order to perform material evaluation fractographic and microscopic methods as well as chemical analysis, were used. Based on results of numerical simulations analysis and data coming from material evaluations the objectives are achieved. In order to prevent future similar problems, the new design of the the half-shafts steering frame was discussed as well.
Findings: It was found that manufacturing and designing of the half shaft system were the main failure reasons. Such open pit machines undercarriages systems are prone to failures. Detailed analyses are required to implement half – shaft systems without risk of break-down. Recommendation is given in the paper for the single shaft system.
Research limitations/implications: Friction in the supporting areas limits horizontal forces acting on safetying of the half-shaft. Sliding and static friction coefficients should be investigated in order to estimate optimal designing rules and correct forces.
Practical implications: Practical implications into designing of half-shafts undercarriage systems and safetyings are given.
Originality/value: The paper provides information backed by test results and evaluation, stating the nexus of causes of the dumping conveyor break-down. The numerical and experimental approaches present relationship between designing and manufacturing. The paper can be helpful for researchers and designers investigating reasons, approach methods or failures preventing methods of similar machines.
Keywords: Cad/Cam; Constructional design; Materials; Metallography

Reference to this paper should be given in the following way:
E. Rusiński, J. Czmochowski, P. Moczko , Half-shaft undercarriage systems – designing and operating problems, Journal of Achievements in Materials and Manufacturing Engineering 33/1 (2009) 62-69.

1. Introduction

There are many researches concerning damage and breakdowns and catastrophes of machines and equipment [8, 9]. Detailed analyses are carried out to determine causes, course and results of such events. Similar cases can be prevented in the future by knowledge gained from such investigations. The source of the problem can be identified by examination of the causes. According to insurance claim this can be also important from the user/owner's point of view. An analysis of the course of such failures allow to determine its causes and results. A block diagram of interdependencies between the activities involved is shown in Figure 1.

Fig. 1. Interdependencies between causes, course and results of breakdown

The course of a break-down is not as important to the user as its causes and results. However to the researcher it is the course of the breakdown, which is most important since it implies conclusions about both the results and the causes. This part of research is also the most interesting from researching point of view. This is presented below for a breakdown of dumping conveyor.

In open pit mines, dumping conveyors form a link in the EBD (excavator, belt conveyor, dumping conveyor) system. The dumping by such machine in opencast lignite mine [4, 6, 7] is shown in Fig. 2.

Fig. 2. Dumping conveyor operating in opencast lignite mine

The overburden which is to be removed from an open pit being mined is transported to dumping conveyor which distributes it on the dump. The dumping conveyor's steerable carriage (Fig. 3) broke down during work in winter conditions. The dumping conveyor's driving system consists of one steerable and two nonsteerable caterpillar units. The steerable caterpillar unit is made up of two crawler frames, a carriage and a steering framet. A schematic of the steerable caterpillar unit is shown in Fig. 4.

The carriage and the shaft have a box structure made of 25 - 30 mm thick plates. The track girder spacing is 5.9 m and the distance between the steering screw and the track girders' axis is 8.5 m. The investigated dumping conveyor has a system of two axle shafts (halfshafts) joining the track girders to the carriage. This design solution is often used in order to reduce the machine's weight. In such machines the halfshafts are usually 3 m long and have a diameter of 500 mm, decreasing to 300 mm inside the carriage. The resulting mass amounts to about 3.5 tons. This design solution requires, however, solid support and protection against slipping out. The mounting of the halfshaft in the carriage box structure is shown in Fig. 5.

Fig. 3. Breakdown of dumping conveyor's steerable carriage

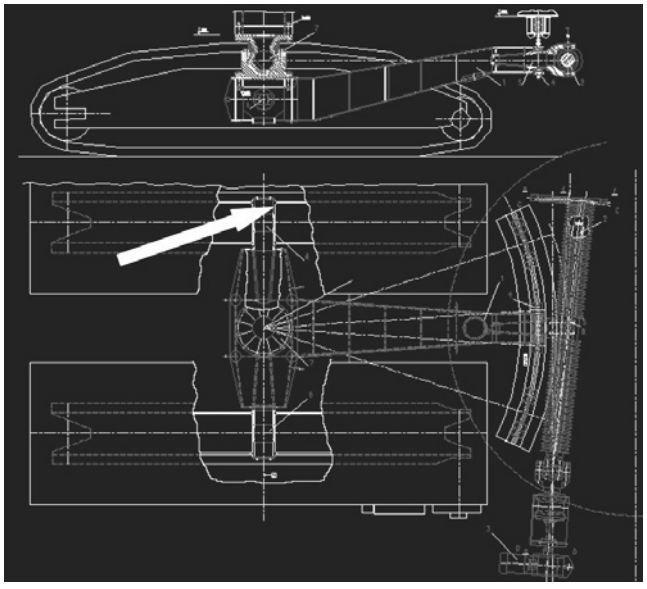

Fig. 4. Schematic of steerable caterpillar unit

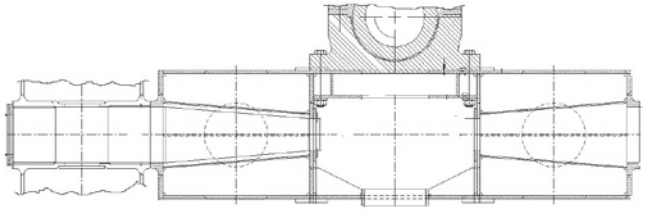

Fig. 5. Halfshaft mounting in carriage structure

Due to damage of half shaft safetying one half-shaft slipped out and caused breakdown of the machine. The track girder of the dumping conveyor after the breakdown is shown in Fig. 6.

Fig. 6. Breakdown of one carriage: results of steerable carriage breakdown

After the dumping conveyor's gantry together with the machine body had been hoisted and the track girder had been removed the damaged end of the halfshaft could be examined. The halfshaft's damaged end with broken off pieces is shown in Fig. 7.

Fig. 7. Damaged halfshaft of steerable carriage

In order to determine the causes of the breakdown the following were carried out:

- an analysis of the forces acting on the steerable unit and on the whole undercarriage in accordance with the current standards [19],
- FEM strength calculations of the steerable unit with the steering shaft,
- defectoscopic tests of the carriage and the halfshafts,
- measurements of carriage plating and halfshaft geometry,
- metallographic examinations of the halfshaft material.

2. Analysis of forces acting on steerable caterpillar unit

The general rules and principles of calculating undercarriages can be found in [6] which analyzes the particular travel resistance components, i.e in details.

- the internal caterpillar track motion resistance,
- the subgrade deformation resistance,
- the climb resistance,
- the curvature travel resistance.

By analyzing the above forces one can determine the loads acting on the particular components of the caterpillar unit. When investigating the causes of the breakdown special attention was paid to the analysis of the forces acting during curvature travel.

According to the current standard for calculating basic surface mining machines DIN 22261-2 calculations should be carried out for the following cases:

- curvature travel (L),
- caterpillar transverse slip (QQ),
- longitudinal dragging (LL),

e.g. when the drive of one of the caterpillar tracks fails. In addition one should include the load from the body at a terrain gradient and wind pressure. The protection systems installed on surface mining machinery do not allow one to activate the turn mechanism when the machine does not move. A turn is possible only during travel. The loads acting on the caterpillar unit during curvature travel are shown in Fig. 8.

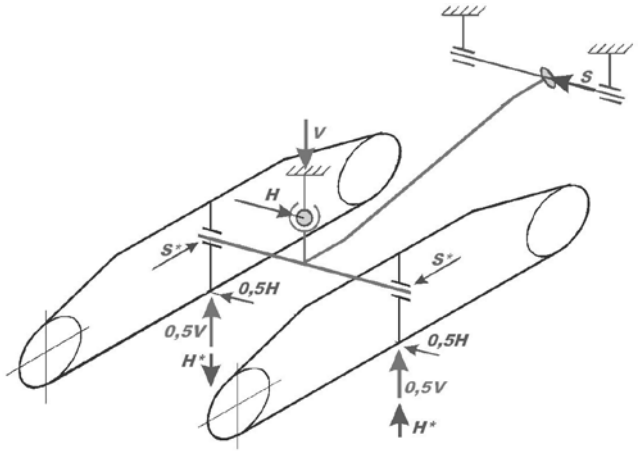

Fig. 8. Forces acting on caterpillar unit during turn

The active forces acting on the undercarriage include:

- Dead weight of body and undercarriage gantry V,
- horizontal force H due to inclination and wind pressure,
- the steering force at the end of the shaft, resulting from the friction of the tracks on the ground

$$S = \mu V \frac{i_R}{R_s} \tag{1}$$

where:
μ – the friction coefficient between the ground and track ($\mu = 0.6$),
i_R – the radius of interia of the caterpillar track contact area,
R_s – the distance between end of steering frame and the crawler frame axis.

In FEM calculations [10, 18] one can substitute supports for the reaction forces.

The described case of loads analyzed in the FEM calculations played a major role in verifying the choice of bearing element cross sections.

3. FEM strength calculations of caterpillar unit carriage shaft

The undercarriage steering frame has a box structure. The numerical model was created using a geometrical model and a discrete shell-beam model. The strength calculations of the undercarriage steering frame were performed for several load cases required by standard [1], with the use of finite element method [3, 5, 17]. Example of strength calculation results [2] presenting the distribution of the Huber-Misses stress in the steering frame for curv travelling load case are shown in Fig. 9.

Fig. 9. Distribution of Huber - Misses stress in dumping conveyor's steering carriage

For all the required cases of loading no stress levels specified by the standard [1] were found to be exceeded. High stresses were observed only in the vertical ribs of the halfshaft's housing.

4. FEM strength calculations of halfshaft end

The loads acting on the halfshaft, particularly on its end where the slip-out protection is situated, were analyzed. Considerable axial forces produced by the side shearing of soil occur during curvature travel. In unfavourable conditions they and the lateral forces due to the gradient and wind pressure may add up. The protection against halfshaft slip out is shown in Fig. 10.

Fig. 10. Halfshaft end - protection against slip out

The plates protecting the halfshaft against slip out were deformed (Fig. 11) as a result of the longitudinal movement of the halfshaft .

Fig. 11. Deformed elements (plates) protecting against halfshaft slip out

Due to the axial clearance of the halfshaft static friction $\mu = 0.09$-0.14 becomes sliding friction $\mu = 0.01$-0.05. One should note that in this case sliding friction should not occur, but it did occur as evidenced by the deformation of the protective plates (Fig. 11). FEM calculations of the halfshaft end were carried out for the most unfavourable case of loading. One should note that because of the very small rounding radius at the bottom of the groove for the protective plates considerable stress concentrations arise under the action of axial forces. The radius is as small as $r = 0.2$ mm (as measured on microsections of the protection). The halfshafts were made of toughened constructional alloy steel 42CrMoS4 whose yield point is Re = 880 N/mm^2 and strength Rm = 1030 N/mm^2. The FEM strength calculations of the halfshaft were performed for two values of the axial force acting on the halfshaft protection: - axial force F = 1393 kN – the axial force at travelling along a curvature with radius R = 60 m with the terrain gradient and wind pressure (HZS (L)) taken into account and with neglected friction ($\mu = 0$) on the halfshaft mounting hubs, - axial force F = 704 kN – the axial force at travelling along a curvature with radius R = 60 m with terrain gradient and wind pressure (HZS (L)) and friction ($\mu = 0.09$) on the halfshaft mounting hubs taken into account.

The first case is rather theoretical since it assumes that total axial force F = 1393 kN acts on the halfshaft's end. But some of the axial force is taken by friction between the hub and the journal at the places of halfshaft mounting. According to standard [1] the coefficient of friction in this case can be assumed at a level of μ = 0.09-0.22. Assuming the less favourable friction coefficient value (μ = 0.09) and knowing the forces in the bearings, the axial force taken by the halfshaft's end was determined to be F = 704 kN.

Figure 12 shows the distribution of Huber-Mises stress determined by FEM calculations [20] for radius r = 0.2 mm and r = 4 mm while the maximum Huber-Mises stresses on the groove's bottom for two values of the axial force transmitted by the halfshaft lug are given in Table 1. The rounding radius of 4 mm was adopted for comparison purposes in order to determine its safe (strength wise) value.

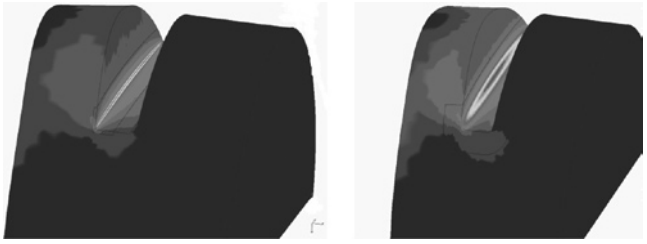

Fig. 12. Distribution of Huber-Mises reduced stress in slide-out protection groove (nonlinear elastoplastic calculations): a) r = 0.2 mm, b) r = 4 mm

Table 1.
Maximum Huber-Mises stresses in analyzed halfshaft end

Calculations	Axial force F [kN]	Rounding radius r [mm]	Reduced stress σ [MPa]	Safety factor δ
without friction	1393	4	822	1.07
		0.2	1080 (1780*))	0.49
with friction	704	4	405	2.17
		0.2	880	1.00

*) a theoretical value for material elasticity in the full load range

The FEM [11] calculations indicate that at the bottom of the groove with radius r = 0.2 mm stresses considerably exceed the yield point. The stresses come down below the yield point at radius r = 4 mm.

5. Metallographic examination of halfshaft

Metallographic examinations were carried on three elements from the fractured caterpillar halfshaft. The elements were denoted as 1, 2 and 3 (Figs. 13 and 14). Naked-eye macroscopic examinations and examinations by means of a stereoscopic microscope at a magnification of 30x were conducted. Also microscopic examinations using a NEOPHOT 32 light microscope and a digital camera were performed.

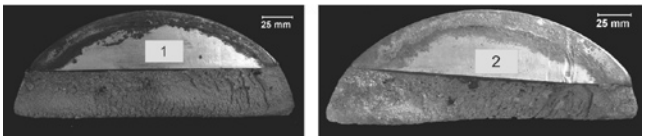

Fig. 13. Fragments broken off caterpillar halfshaft – element 1 and 2

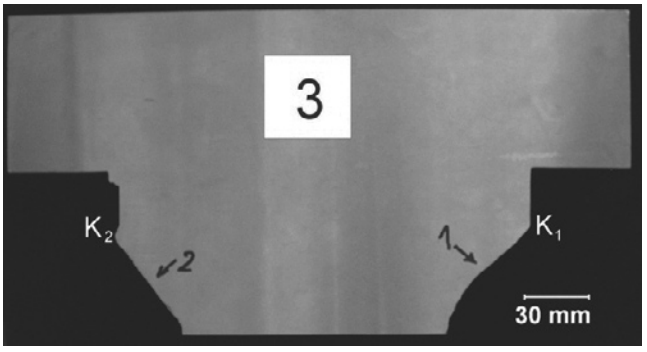

Fig. 14. Piece cut out from damaged halfshaft cross section – element 3

The macroscopic examinations showed fractures originating in the caterpillar half-shaft. The fractographic investigations showed that the fractures had fatigue fracture features, including a temporary coarse-grained brittle zone (Figs. 15 and 16). In element 1 the fatigue zone area is located near edge AC and it takes up about 2% of the fracture area. The fatigue zone area in element 2 is located near edge EG, occupying about 4% of the fracture area (Fig. 14). The fractures were locally coated with corrosion products. The fatigue zones have a lenticular shape, most wide close to the middle of edges AC and EG in the investigated elements [12, 16]. The places are denoted as S1 and S2 for respectively elements 1 and 2. The fatigue zone in point S1 is about 3 mm wide against the temporary zone width of about 65 mm while in point S2 it is about 6 mm wide against the temporary zone width of about 60 mm (Fig. 15). In the case of element 1, the first fatigue zone area is located by edge A and the second one at a distance of about 20 mm from edge C. Similarly in element 2 one fracture fatigue zone area is located directly at edge E while the other at a distance of about 10 mm from edge G. Such a fatigue fracture structure indicates that the largest stresses occur in the medial part of the groove towards points A and C (element 1) and E and G (element 2).

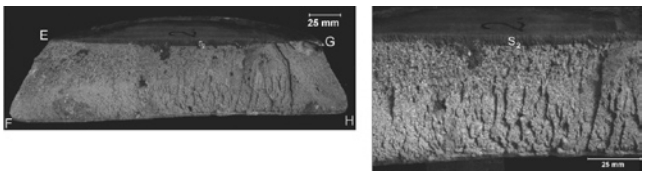

Fig. 15. General view of surface of fracture with marked edges. Symbol S2 marks widest fracture fatigue zone area

It was found that both fractures had been initiated at the place where the cross section changes. The fatigue zone is located along the undercuts denoted by symbols K1 and K2 in Fig. 14. The fracture of element 1 ran parallel to edge AC and at an angle of 45 deg. to the halfshaft's longitudinal symmetry axis by edge GH. The angle gradually increases to-wards edge EF, reaching 60 deg.. This indicates that in element 1 the fracture of the half-shaft groove resulted from the action of shearing forces and bending moments on it. As a result of damage to element 1 an additional bending moment was produced (as one point of support was removed) whereby the direction of fracture propagation changed in element 2, as evidenced by the clear plastic deformation in point G, which probably occurred in the final stage of fracturing (Fig. 16).

Fig. 16. Element 2. Magnified fragment from Fig. 15 (visible plastic deformation in point G)

The small area of the fatigue zone in comparison with that of the temporary zone is evidence of great strain of the halfshaft material. This means that either too low safety factors were adopted or the allowable stress was considerably exceeded during operation. Also improper heat treatment of the element's structural material could be the cause. The most likely places of fracture initiation are points A and C (element 1) and E and G (element 2) where a local stress concentration might have occurred because of the change in the cross section. The fact that the fracture occurred in the middle section of edges AC and EG may suggest either nonuniform distribution of stresses (surface pres-sures) in the groove or a manufacturing or structural notch. The nonuniform stress pattern in the halfshaft groove could also be due to the faulty fabrication of the grooves, and also of the plates (e.g. their clamping surfaces not being flat and parallel).

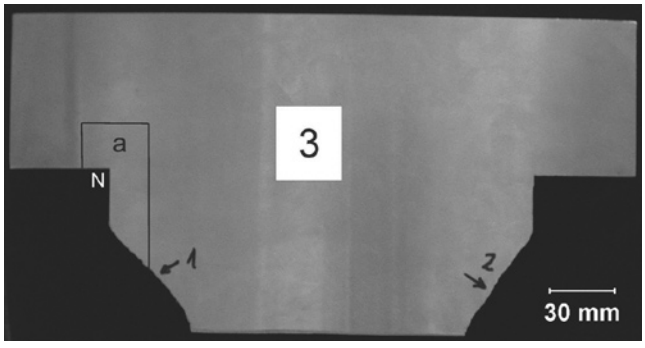

Fig. 17. Place (determined by macroscopic examinations) where specimens for further metallographic studies were taken

The signs of wear on the clamping surfaces indicate that the surface pressures were distributed on the groove's circumference and not over its whole surface. This distribution of clamping stresses explains the lenticular shape of the fatigue zone: since the clamping forces are uniformly distributed on the circumference, the maximum bending moments produced by them occurred in the groove's middle part in the region of points S1 and S2. The place from which the specimens were taken is shown in Fig. 17.

On both sides of specimen a the radius on the edge of the halfshaft groove for sliding in the protective plates was measured in the place marked N in Fig. 18. A transition with curvature radius r=0.2 mm was found. This radius is too small to be a manufacturing radius.

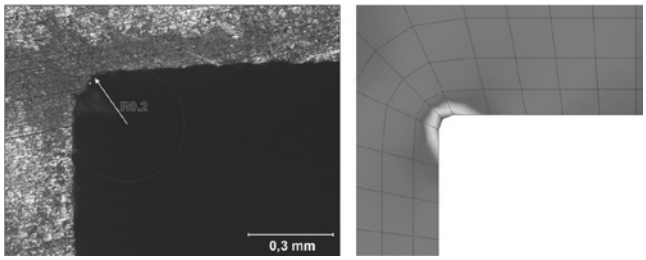

Fig. 18. Location of halfshaft groove; a) groove edge curvature radius r = 0.2 mm on specimen's left side, b) plastic strain zone on groove's bottom

Microscopic examinations were carried out on unetched and etched (with Mi1Fe re-agents) microsections. The results of the examinations are shown as microphotographs in Figs. 19-22.

In the unetched microsections non-metallic inclusions, mainly in the form of sulphides uniformly distributed over the whole surface of the specimen along the direction of plastic forming (Fig. 19), were found.

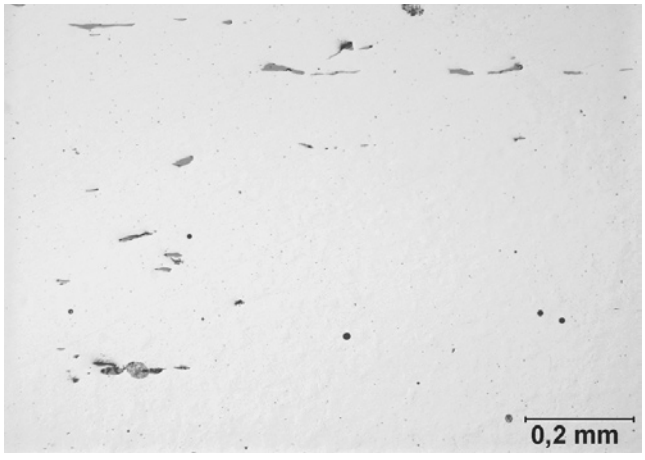

Fig. 19. Non-metallic inclusions uniformly distributed over whole surface of micro-section along direction of plastic working. Unetched condition. Light microscopy

After etching with Mi1Fe a pearlitic-ferritic structure (locally in the form of the Widmanstätten structure) was observed (Fig. 21).

Such a microstructure is the result of local inhomogeneity in chemical composition, caused by improper heat treatment and plastic forming and incomplete reforging of the steel because of the considerable thickness of the component. Consequently, the material's mechanical properties might have deteriorated [15].

The examinations also showed a crack originating from the groove's edge, running parallel to the cross section change edge at an angle of 45deg to the shaft's axis and running along the boundaries of ferrite and pearlite grains (Fig. 22).

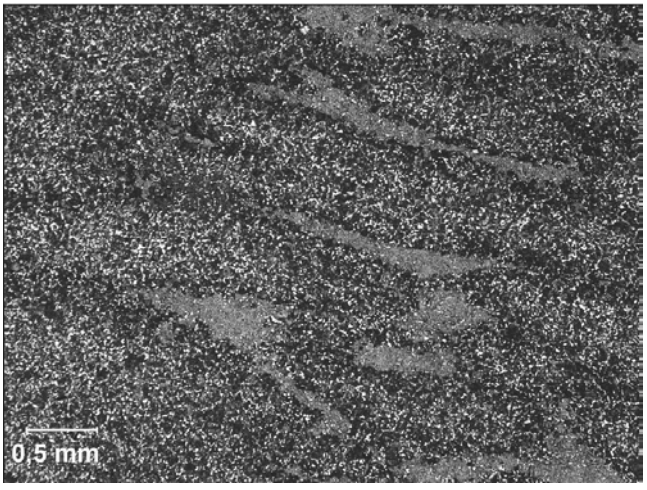

Fig. 20. Inhomogeneous pearlitic-ferritic structure. Etched condition. Light micros-copy

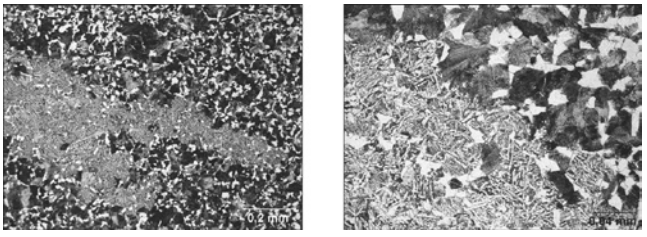

Fig. 21. Etched condition. Light microscopy: a) inhomogeneous pearlitic-ferritic mi-crostructure with features of Widmanstätten structure, b) magnified fragment

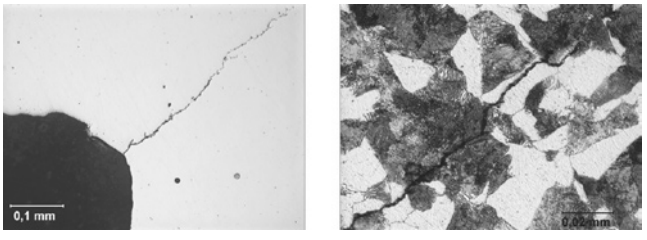

Fig. 22. Edge of lock groove. Light microscopy: a) visible crack initiated in area where cross section changes – unetched condition, b) magnified fragment of area in etched condition, visible crack running along boundaries of ferrite and pearlite grains

6. Conclusions

The FEM analyses of the caterpillar unit and of the halfshaft end showed that the main cause of the breakdown was the way in which the halfshaft had been protected against slipping out. The fractures in the caterpillar support halfshaft lock are of the fatigue type: the temporary part is brittle and coarse-grained. The fatigue zones were initiated at the place where the cross section changes. They extend from the groove's edge into the material at an angle of about 45deg to the halfshaft's symmetry axis and have a lenticular shape which is widest near the middle of the groove's edge. The fatigue zone area in specimen 1 amounts to 2% and in specimen 2 to about 4%. This fatigue fracture structure suggests that the largest stresses occurred in the groove's medial part.

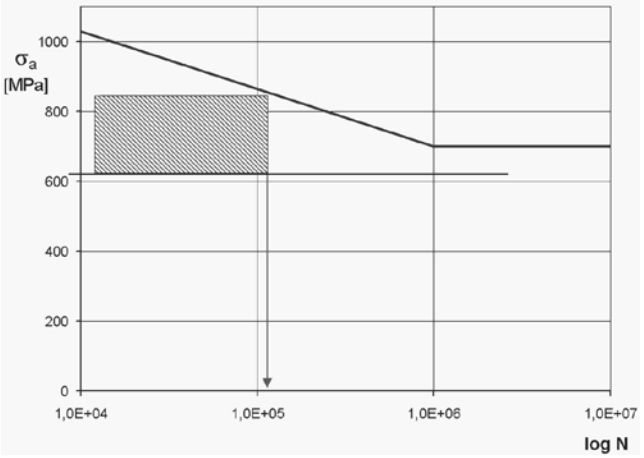

Fig. 23. Wöhler diagram for steel 40HM with marked limited fatigue strength region for radius r = 0.2 mm in halfshaft grooves

Due to the low ratio of fatigue zone area to remaining zone area a considerable effort of the structure or the use of very low safety factors could have been the case. Pearlitic-ferritic structure with locally occurring Widmanstätten structure was observed in the investigated element. These features might have resulted in the deterioration of the material's mechanical properties. Such a structure indicates that the element was not properly heat treated. Microscopic examinations of element 3 revealed the presence of cracks (Fig. 21) indicating the onset of fatigue fracture. The cracks were initi-ated at the place at the groove's bottom where the cross section changes and they ex-tend into the material at angle of about 45deg parallel to the whole edge of the specimen taken from the element. The examinations showed that the slip-out protection had not been properly designed and made. The direct cause of the breakdown was the too small rounding radius of the groove's bottom (r = 0.2), leading to fracture, sliding out of the halfshaft and the breakdown of the dumping conveyor. A fatigue analysis of the groove's bottom showed that the halfshaft material was in the range of limited fatigue strength (Fig. 22). Hence it is concluded that the adopted protection is not good for this system of fixing the halfshafts. A much better solution is an annular protection with a properly large rounding radius of the halfshaft groove. The undercarriage system consisting of two

halfshafts is advantageous from the fabrication and weight points of view. An alternative could be a single-shaft design in which the slide-out protection is much simpler (vertical protection in the form of an additional shaft). But this system would be much heavier (hollow shafts could be employed to reduce the weight) and more expensive.

Since many breakdowns of two-shaft undercarriages have been reported it can be concluded that such systems require more care in their design as compared with single-shaft systems. It can be helpful here to run numerical simulations to identify the weak points of the design. This approach was adopted in the present research. Also friction forces at the places where the halfshafts are supported play a significant role. Depending on the kind of friction (static or sliding) they can reach different magnitudes. In many cases, such loads determine the safety of operation of the undercarriage. But the magnitudes of the forces have not been precisely identified yet. Therefore further experimental re-search is needed to make the design of such systems more accurate.

References

[1] J. Brändlein, Elastische Verformungen der Gehäuse beeinflussen die Wälzlagerung, Maschienenmarkt 56, 1980.

[2] Ch.R. Brooks, A. Choudhury, Failure analysis of engineering materials, McGraw-Hill, New York, 2002.

[3] R.D. Cook, D.S. Malkus, M.E. Plesha, R.J. Witt, Concepts and Applications of Finite Element Analysis, Fourth Edition, John Willey, New York, 2001.

[4] D. Dudek, KRUPP-Schaufelradbagger SchRs-4600 in polnischen Tagebauen. Braunk. Tagebautech. Bd 38 H. 1/2, 1986 (in Polish).

[5] J.M. Dulieu-Barton, M.J. Brennan, Damage assessment of structures, Proceedings of the 5th International Conference "Damage Assessment of Structures" DAMAS 2003, Southampton, UK, 2003.

[6] W. Durst, W Vogt, Schaufelradbagger. Trans Tech Publications, 1989 (in German).

[7] H. Hawrylak, R. Sobolski, Open cast mining machines, Publisher „Śląsk", Katowice, 1967 (in Polish).

[8] E. Rusinski, J. Czmochowski, P. Moczko, Numerical and experimental analysis of a mine's loader boom crack, Journal of Achievements in Materials and Manufacturing Engineering 17 (2006) 273-276.

[9] E. Rusinski, J. Czmochowski, P. Moczko, Failure reasons investigations of dumping conveyor breakdown, Journal of Achievements in Materials and Manufacturing Engineering 23/1 (2007) 75-78.

[10] E. Rusiński, J. Czmochowski, T. Smolnicki, Advanced Finite Element Method for Load-carrying Structures of Machines, Wroclaw University of Technology Press, Wroclaw, 2000 (in Polish).

[11] E. Rusinski, A. Kopczynski, J. Czmochowski, Tests of thin-walled beams joined by spot welding, Journal of Materials Processing Technology 157-158 (2004) 405-409.

[12] J. Schijve, Fatigue of structures and materials, Kluwer Academic Publishers, Jun 2001.

[13] B. Schlecht, Modern Drive Technology for the Mining- and Minerals-Industry, Bulk Solids Handling 17/1 (1997) 89-96.

[14] B. Schlecht, Effektive Überlastsicherung in Schaufelradantrieben, Braunkohle 50/1 (1998) (in German).

[15] C.W. Wegst, Key to Steel, Verlag Stahlschlussel Wegst, Marbach, 2001 (in German).

[16] B. Wurm, Ermüdungsuntersuchungen an scharf gekerbten Proben. Zugl., Dresden, VDI-Verl., Düsseldorf, 2000 (in German).

[17] Y. Zhang, D. Redekop, Shell element simulation of the push method of tube bending, Journal of Achievements in Materials and Manufacturing Engineering 17 (2006) 301-304.

[18] O.C. Zienkiewicz, R.L. Taylor, The Finite Element Method, Volume 2: Solid Mechanics, Fifth Edition, Butterworth-Heinemann, 2000.

[19] DIN/22261-2 – Bagger Absetzer und Zusatzgeräte in Braunkohlentagebauen, Teil 2: Berechnungsgrundlagen (in German).

[20] I-DEAS Master Series, Mechanical CAE/CAD/CAM Software, Structural Dynamics Research Corporation, Milford, 2000.